Available online at www.sciencedirect.com
SCIENCE DIRECT
Earth and Planetary Science Letters 242 (2006) 286–301
EPSL
www.elsevier.com/locate/epsl

Methane-rich fluid inclusions from ophiolitic dunite and post-collisional mafic–ultramafic intrusion: The mantle dynamics underneath the Palaeo-Asian Ocean through to the post-collisional period

Wei Liu *, Pan Xiao Fei

State Key Laboratory of Lithospheric Evolution and Key Laboratory of Mineral Resources, Institute of Geology and Geophysics, Chinese Academy of Sciences, P. O. Box 9825, Beijing 100029, China

Received 1 June 2005; received in revised form 30 November 2005; accepted 30 November 2005
Available online 26 January 2006
Editor: E. Boyle

Abstract

The protracted development history of the Palaeo-Asian Ocean starting from ~1000 Ma to ~320 Ma, and continuation of mantle-derived magmatism right through the post-collisional period as manifested by the widespread mafic–ultramafic intrusion and alkaline–peralkaline granite suggest a vigorous, long-running mantle dynamo. Using the micro-laser Raman spectrometer, we analyzed olivine- and plagioclase-hosted fluid inclusions from ophiolitic dunite, Kudi of the western Kunlun Range, and post-collisional mafic–ultramafic intrusions of the Xiangshan and the Huangshandong, eastern Chinese Tienshan Mountains. Our results show that fluids brought from the mantle by these rocks are rich in H_2O and CH_4 with variable amounts of N_2. Estimation of the redox state, pressure and depth of formation for the melt–CH_4–H_2O+N_2 fluid systems from the 3 rock suites of the Xinjiang, and comparison of these parameters with those of the peridotite–fluid parageneses for the sub-cratonic upper mantle give meaningful results. These fluids were formed in the asthenosphere, were originally CH_4–N_2-rich, primordial mantle fluid, but have been progressively diluted with H_2O and become oxidized by repeated subduction of oceanic slab. We propose that repeated redox melting in the mantle due to dilution of CH_4 with H_2O and oxidation caused formation of the long-lived Palaeo-Asian Ocean, brought about extensive intrusion of mafic–ultramafic complexes and alkaline–peralkaline granites right through the post-collisional period, and, consequently, resulted in significant Phanerozoic continental growth in the Central Asian Orogenic Belt. Rise of atmospheric O_2 and the Earth's major oxidation occurred at about 2.4 to 2.2 Ga. Oxidation of the Earth's mantle promoted the mantle melting and magma input to the crust, resulting in major continental growth after 2.5 Ga. However, much-postponed oxidation of the primordial mantle underneath the Central Asian Orogenic Belt led to significant continental growth in the Phanerozoic times.

Keywords: CH_4–H_2O+N_2 fluid inclusion; dunite; mafic–ultramafic intrusion; redox melting; Palaeo-Asian Ocean

1. Introduction

There existed a long-lived Palaeo-Asian Ocean (PAO) between continental blocks of Baltica, Siberia, and central Asia (Tarim, Kazakhstan, North China) from

* Corresponding author. Tel.: +86 1 010 62007557.
E-mail address: liuw@mail.igcas.ac.cn (W. Liu).

0012-821X/$ - see front matter © 2005 Elsevier B.V. All rights reserved.
doi:10.1016/j.epsl.2005.11.059

the terminal Mesoproterozoic to the middle Paleozoic [1–8]. The final closure of this ocean in the Late Paleozoic led to the formation of the Central Asian Orogenic Belt (CAOB) [9]. Between ~1000 and 510 Ma, the Palaeo-Asian Ocean had a complex active Siberian margin on the east and a passive Kazakhstan–Tarim margin on the west (present-day reference frame) [10]. After 510 Ma, however, it showed an architectural asymmetry in the opposite sense with system of volcanic arcs and marginal basins in the west and an Andean–Cordilleran margin in the east [10]. Numerous but small oceanic basins appeared in the western margin of the Palaeo-Asian Ocean [11,12].

2. Paleozoic ophiolite suites in the Xinjiang of China

As shown in Fig. 1, Paleozoic ophiolites are widespread in the Xinjiang of China. The Paleozoic tectonic evolution of the northern Xinjiang has been reconstructed largely based on geochronological and palaeontological constraints on ophiolites. These include the Pb–Pb isotopic dating on sphene and plagioclase [15] and the discovery of radiolarian fossils [11,16] from the Tangbale ophiolite, the discovery of mid-Ordovician fossils from the Hongguleleng ophiolite [11], whole-rock Sm–Nd isotopic dating of harzburgite and dunite [17] and SHRIMP zircon U–Pb dating of plagiogranite [18] from the Aermantai ophiolite, and the discovery of Ordovician radiolarian fossils [19] from the suite, the discovery of Silurian or pre-Silurian radiolarian fossils in cherts from the Mayile ophiolite [16], discovery of the Early to Middle Devonian fossils from the Darbut ophiolite [11] and Sm–Nd isotopic dating of gabbroic cumulate from the suite [20], discovery of the Early to Middle Devonian micro-fossils in cherts from the Kerameili ophiolite [21], zircon U–Pb dating of trondjemite from the Kekesentao–Qiaoxiahara–Kuerti ophiolite belt [22], and discovery of the Late Devonian to Early Carboniferous micro-fossils in the Bayingou ophiolite from the northern Chinese Tienshan Mts. [11]. It was established that, in the northern Xinjiang during the Paleozoic, the Late Cambrian to Early Ordovician Tangbale–Mayile–Hongguleleng–Aermantai ophiolite complexes occur in the center, the Early to Middle Devonian Darbut–Kerameili complexes and the Late Devonian to Early Carboniferous northern Chinese Tienshan complexes in the south, and the Middle to Late Devonian Kekesentao–Qiaoxiahara–Kuerti complexes in the north [23]. The Paleozoic ophiolites of the northern Xinjiang are oceanic fragments that show affinities to mid-ocean ridge basalt, oceanic island basalts, and island arc basalts [23]. These geochemical signatures indicate a source component from the lower mantle [24]. In addition, the Carboniferous adakite, high-Mg andesite, and Nb-enriched arc basalt in the Alataw Mountains [25], and adakite in association with the ophiolite-related volcanics in the Kekesentao–Qiaoxiahara–Kuerti complexes [26] were generated by melting of young subducting oceanic slab at abnormally high temperatures [27]. The ophiolite-associated sedimentary sequences and subduction-related volcanics show an evolutionary trend from intra-oceanic setting in the Early Paleozoic to marginal setting in the Late Paleozoic. Subduction-accretion terminated in the terminal Early Carboniferous [28]. Nevertheless, continental growth via vertical accretion or mantle input commenced soon following termination of the subduction-accretion, indicating that the mantle dynamo was still running.

As shown in Fig. 1, in the western Kunlun and the Altyn Tagh and the eastern Kunlun on the southern margin of the Tarim block, there was in Ordovician time oceanic crust, south-dipping intra-oceanic subduction and island arcs, and in Late Devonian to Early Carboniferous time radiolaria-bearing carbonate and/or clastic sediments that overly arc-type lavas and pyroclastic rocks [14,29,30]. As shown in inset B of Fig. 1, the arc ophiolite is characterized by harzburgite-depleted mantle overlain by lavas that show close affinities to island-arc tholeiite or oceanic island basalt [31]. These features again suggest a source component from the lower mantle [24]. These ophiolites constitute a Mid-Paleozoic suture zone that extends from the Pamir syntaxis in the west to the Altyn Tagh and the East Kunlun Range in the east (Fig. 1). In consideration of the close spatial and temporal relations to those occurring in the northern Xinjiang, we regard these ophiolites as the southernmost portion of the Palaeo-Asian ocean.

3. Post-collisional mafic–ultramafic intrusions and alkaline–peralkaline granites in the Xinjiang

As shown in Fig. 1, there occur many mafic–ultramafic intrusive complexes in the Xinjiang. The Kalatongke complex, eastern Junggar, and the Huangshan–Jingerquan complex belt, eastern Chinese Tienshan Mountains, have been extensively studied as they host important Cu–Ni sulfide ore deposits. Rb–Sr, Sm–Nd [32] and recent SHRIMP zircon U–Pb [33] isotopic dating has yielded consistent ages in the range 298–285 Ma for intrusion of the Kalatongke complex. Recent Re–Os [34] and SHRIMP zircon U–Pb [33] isotopic dating has yielded ages of 282±20 Ma and 274±3 Ma (MSWD=1.35), respectively, for intrusion of the

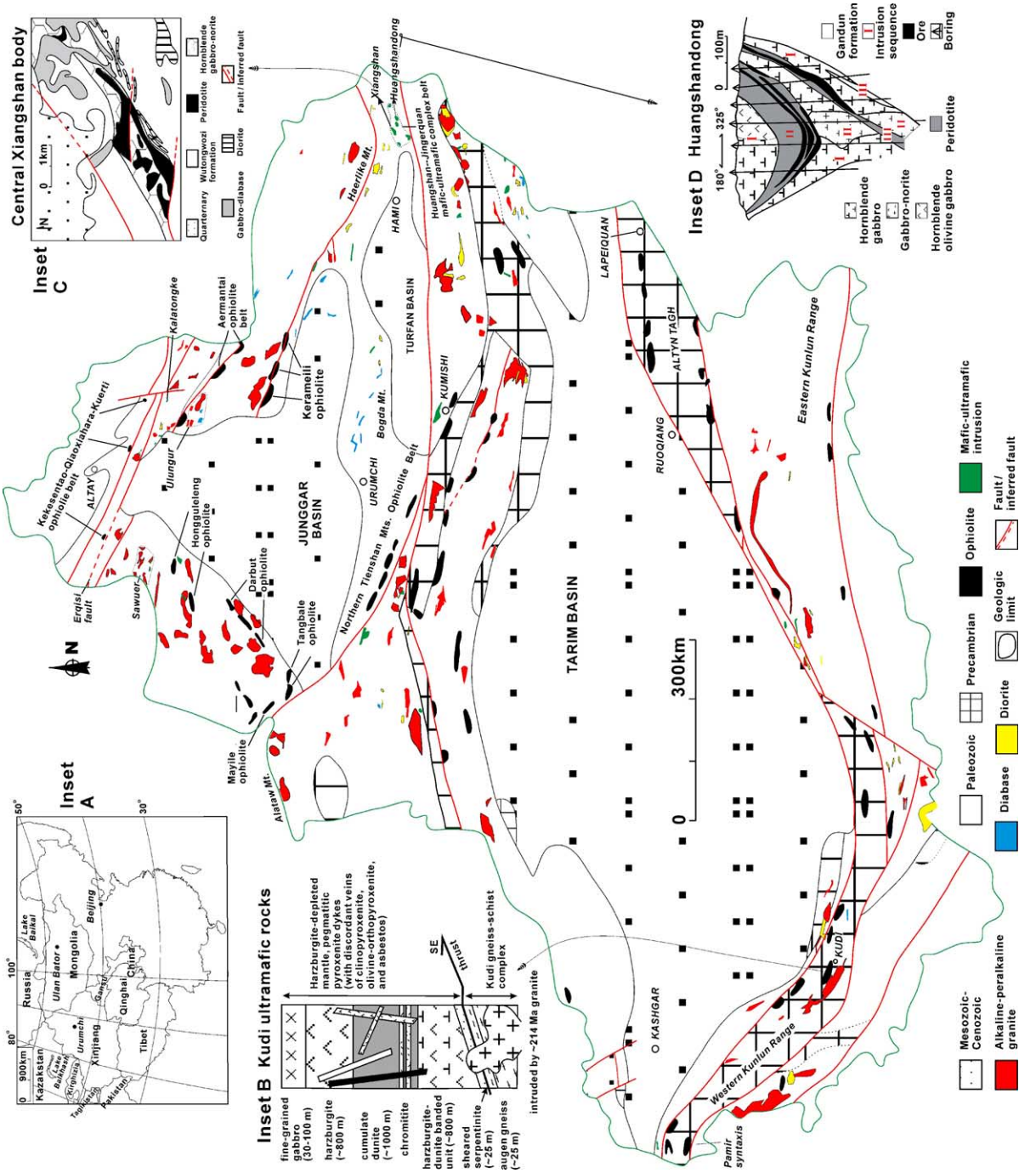
Inset A
Inset B Kudi ultramafic rocks
Inset C
Central Xiangshan body
Inset D Huangshandong
TARIM BASIN
TURFAN BASIN
JUNGGAR BASIN
Eastern Kunlun Range
Western Kunlun Range
Pamir syntaxis
ALTYN TAGH
Keksentao-Qiaoxiahara-Kuerti ophiolite belt
Aermantai ophiolite belt
Kerameili ophiolite
Honggulelenng ophiolite
Darbut ophiolite
Tangbale ophiolite
Mayile ophiolite
Northern Tienshan Mts. Ophiolite Belt
Huangshan–Jingerquan mafic-ultramafic complex belt
Haerlike Mt.
Bogda Mt.
Alataw Mt.
Erqisi fault
Sawuer
Ulungur
Kalatongke
Xiangshan
Huangshandong
KUMISHI
HAMI
URUMCHI
LAPEIQUAN
RUOQIANG
KASHGAR
KUDI
Harzburgite-depleted mantle, pegmatitic pyroxenite dykes (with discordant veins of clinopyroxenite, olivine-orthopyroxenite, and asbestos)
fine-grained gabbro (30-100 m)
harzburgite (~800 m)
cumulate dunite (~1000 m)
chromitite
harzburgite-dunite banded unit (~800 m)
sheared serpentinite (~25 m)
augen gneiss (~25 m)
SE
Intrusive
Kudi gneiss-schist complex
intruded by ~214 Ma granite
Quaternary
Witongwozi formation
Gabbro-diabase
Peridotite
Diorite
Hornblende gabbro-norite
Fault / inferred fault
Gandun formation
Intrusion sequence
Ore
Boring
Hornblende gabbro
Gabbro-norite
Hornblende olivine gabbro
Peridotite
Mesozoic-Cenozoic
Alkaline-peralkaline granite
Paleozoic
Precambrian
Diabase
Ophiolite
Diorite
Geologic limit
Mafic-ultramafic intrusion
Fault / inferred fault
300km
Russia
Kazakstan
Mongolia
Lake Baikal
Ulan Bator
Beijing
Qinghai
China
Tibet
Kirghizia
Tadjikistan
Pakistan
Kinjiang
Gansu
Uruimchi

Huangshandong from the Huangshan–Jingerquan complex belt, while conventional zircon U–Pb [35] isotopic dating yielded an age of 285 ± 1.2 Ma for intrusion of the Xiangshan from the same belt. The isotopic ages confirm that these mafic–ultramafic complexes were intruded in the post-collisional relaxation or extensional period. The $\varepsilon_{Nd}(t)$ values for the Kalatongke and the Huangshandong intrusions are averaged at +5.60 and +7.29 [33], respectively, indicating a mantle derivation. It is interesting to note that alkaline–peralkaline granites in the Xinjiang also intrude in the post-collisional period, though slightly earlier than the mafic–ultramafic intrusions. For instance, the Ulungur peralkaline granite belt that is near to the Kalatongke mafic–ultramafic complex and overlaps the former Aermantai ophiolite belt, and the Kerameili–Haerlike alkaline–peralkaline granite belt that is close to the Huangshan–Jingerquan mafic–ultramafic complex belt and overlaps the former Kerameili ophiolite belt intruded during 306–270 Ma [17,36–40]. Recent SHRIMP zircon U–Pb dating reveals that alkaline–peralkaline granites in the Sawuer Mts., western Junggar, were intruded during 297.9–290.7 Ma (T.F. Zhou, unpublished data, personal communication). Recent SHRIMP zircon U–Pb dating shows that diorites in the Haerlike and the Bogda Mountains, eastern Xinjiang, were intruded during the post-collisional period [41]. Moreover, the widespread Early Permian volcanics in the Sawuer and the Ulungur exhibit a bimodal distribution and an evolutionary sequence from andesite–trachybasalt–rhyolite–andesite–basaltic rocks. The alkaline–peralkaline granites in the Xinjiang and the whole Central Asian Orogenic Belt show positive or high $\varepsilon_{Nd}(t)$ value, young T_{DM} age, and low initial $(^{87}Sr/^{86}Sr)_t$ ratios (e.g. [40,42–45]), indicating addition of juvenile crust via basaltic underplating under a lithospheric extensional regime [45]. In addition, production of the Permian adakites in the Awulale, western Chinese Tienshan Mountains, also calls for basaltic underplating resulting in overthickened lower crust [46]. We emphasize that, in addition to the Cu–Ni sulfide deposits, a great majority of the gold deposits in the Xinjiang were deposited in the Late Carboniferous to Permian times, broadly concurrent with the post-collisional magmatism. Gold deposits in the southern Altay Mts. and along the Erqisi fault zone were dated at 317–269 Ma [32] and at 292.8–289 Ma using the $^{40}Ar/^{39}Ar$ method [47]. The Hatu gold deposit in the western Junggar was dated at 290–288 Ma [48]. Ages of the gold deposits in the eastern and the western Chinese Tienshan Mts. range from 300 to 244 Ma and from 344 to 277 Ma, respectively [32]. Fluid inclusion and H, O, S, Pb, He, and Ar isotopic studies show strong magmatic signature or mantle affinity for the ore-forming fluid from many of these post-collisional gold deposits [49–51].

In summary, the prolonged – but limited – development history of the Palaeo-Asian Ocean, the repeated appearance of volcanic arcs and marginal basin systems and their accretion and collision onto continental blocks, the alternation from an active to a passive continental margin, and continuation of mantle-derived magmatism right through the post-collisional period all call for a vigorous, long-running mantle dynamo.

Fluid brought from the mantle by the ophiolitic dunite and post-collisional mafic–ultramafic intrusion can provide important information on the redox state, source reservoir, and melting conditions of the mantle before and after final closure of the Palaeo-Asian Ocean. Determination of these conditions can help to unravel the problem of protracted mantle melting and magma input to the crust that have given rise to the development of the Palaeo-Asian Ocean, post-collisional magmatism, and hydrothermal–mineralization throughout the Central Asian Orogenic Belt. In the past 3 yrs, we have made endeavor to find fresh rocks free from alteration from the ophiolitic ultramafic rocks and post-collisional mafic–ultramafic intrusions in the Xinjiang, China; most of them have been altered to various extents. Nevertheless, we have tried to find rather fresh dunite from Kudi, the western Kunlun Range, and have screened out relatively fresh rocks from the central Xiangshan and the Huangshandong mafic–ultramafic intrusions, the Huangshan–Jingerquan belt (Fig. 1). In this study, we analyzed the gaseous species from fluid inclusions hosted by these rocks using the micro-laser Raman spectrometer, in an attempt to determine the redox state, source reservoir, and melting conditions in the mantle underneath the Palaeo-Asian Ocean through to the post-collisional period.

Fig. 1. Geological sketch map of the Xinjiang of China showing the distribution of Paleozoic ophiolite, and post-collisional intrusions that include mafic–ultramafic complex, diabase, diorite, and alkaline–peralkaline granite, adapted from the XBGMR [13]. The ophiolite is exaggerated. Inset A shows the location of the Xinjiang within the outline of China, and its geographic relations to the neighboring provinces or autonomous region in China and neighboring countries of Central Asia. Inset B shows the stratigraphic column of the Kudi ophiolite, western Kunlun Range, which is thrust over the Kudi gneiss–schist complex and intruded by a 214 Ma granite, adapted from Xiao et al. [14]. Not to scale. Inset C shows the well-developed rock facies within the central body of the Xiangshan mafic–ultramafic intrusion, Huangshan–Jingerquan complex belt. Inset D is the No. 8 prospecting profile of the Huangshandong mafic–ultramafic intrusion, Huangshan–Jingerquan complex belt, showing the three intrusion sequences.

4. Geological setting and petrography of studied samples

The Kudi ophiolite in the western Kunlun Range marks the western segment of the Mid-Paleozoic suture zone on the southern margin of the Tarim block [52,53]. From bottom to top, the Kudi ophiolite includes the oceanic crust (ultramafic rocks), an intra-oceanic arc comprising basalt–andesite–tuff–agglomerate, and the arc- or ophiolite-derived turbidite of two generations containing Late Ordovician–Silurian and Late Devonian–Early Carboniferous radiolarians [52–54]. Xiao et al. [14] interpreted the sequence as a substrate of ocean-floor (ophiolitic ultramafic–mafic rocks) overlain by an Ordovician–Silurian intra-oceanic, suprasubduction arc, which is further overlain by a Late Devonian–Early Carboniferous turbiditic forearc basin. As shown in inset B of Fig. 1, stratigraphically from bottom to top the Kudi ultramafic rock is composed of sheared serpentinite on the basal thrust, layered harzburgite–dunite, layered dunite with chromitite, and harzburgite with fine-grained gabbro [14]. The dunite is rather fresh and has coarse- and fine-grained layers plus layers of clinopyroxenite, and is traversed by discordant veins of clinopyroxenite, olivine–orthopyroxenite and asbestos. As shown in Fig. 2(a), sample KD was collected from the fine-grained layer of dunite, and consists of olivine (95% by the volume) and a small amount of pyroxene (<5%). The olivine (0.25–1 mm in grain size) and pyroxene (0.2–2 mm) are rather fresh with little alteration even along parting (Fig. 2(a)). As shown in Fig. 2(b), the studied fluid inclusions in KD occur along three growth planes of olivine. These fluid

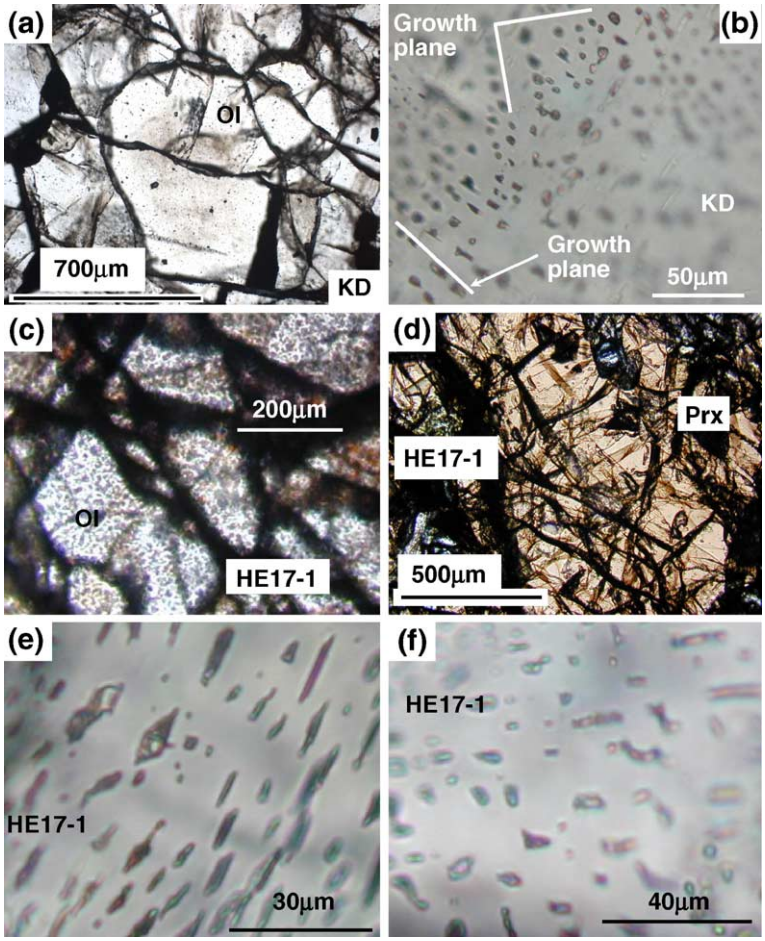

Fig. 2. Photomicrographs showing the petrographic feature and the olivine-hosted fluid inclusions for the dunite sample KD, Kudi ophiolite ((a) and (b)), and the peridotite sample HE17-1, Huangshandong mafic–ultramafic intrusion ((c)–(f)). The fresh olivine in (a) and the occurrence of fluid inclusions along three growth planes of olivine (b) are noteworthy. Abbreviations: Ol—olivine; Prx—proxene. All photomicrographs taken with the plain light.

inclusions were trapped during crystallization of olivine and, therefore, represent the mantle fluid.

The central Xiangshan and the Huangshandong plutons are the two typical intrusions from the Huangshan–Jingerquan mafic–ultramafic complex belt (Fig. 1). As shown in inset C of Fig. 1, the central Xiangshan body intrudes the basic lava and baschtauite of the Late Carboniferous Wutongwozi formation, and comprises peridotite, gabbro–norite, diorite and gabbro–diabase. Gabbro–norite constitutes the main body of the pluton, whereas peridotite occurs discontinuously within the pluton. Gabbro–diabase and diorite occur peripherally to the main body and cut the country rock. However, different rock facies are transitional without a clear-cut boundary. The studied samples Xis1, Xis2, and Xis4 were collected in the tunnel from the relatively fresh gabbro–norite. As shown in Fig. 3(a)–(c), the gabbro–norite is composed of plagioclase (63–70%) that is dominantly labrador with subordinate bytownite, pyroxene (16–20%) that includes hypersthene and diopside, olivine that is chrysolite (3–6%), pargasitic hornblende (5–10%), biotite (1–3%), and opaque minerals. Megacrysts of poikilitic hornblende are abundant in all the rock facies, and have grown around plagioclase and olivine (Fig. 3(b)), indicating that the parent magma is rich in water. Plagioclase-hosted fluid inclusions occur in isolation (Fig. 3(e)) or in group without obvious orientation (Fig. 3(d)). However, fluid inclusion trail is parallel to the grain boundary of plagioclase (Fig. 3(f)). Some fluid inclusions occur within the plagioclase that is surrounded by the poikilitic hornblende (Fig. 3(c)). Therefore, the plagioclase-hosted fluid inclusions are primary or pseudo-secondary [55]. As the crystallization of hornblende marks the extensive exsolution of magmatic fluid from the magma, those pseudo-secondary fluid inclusions

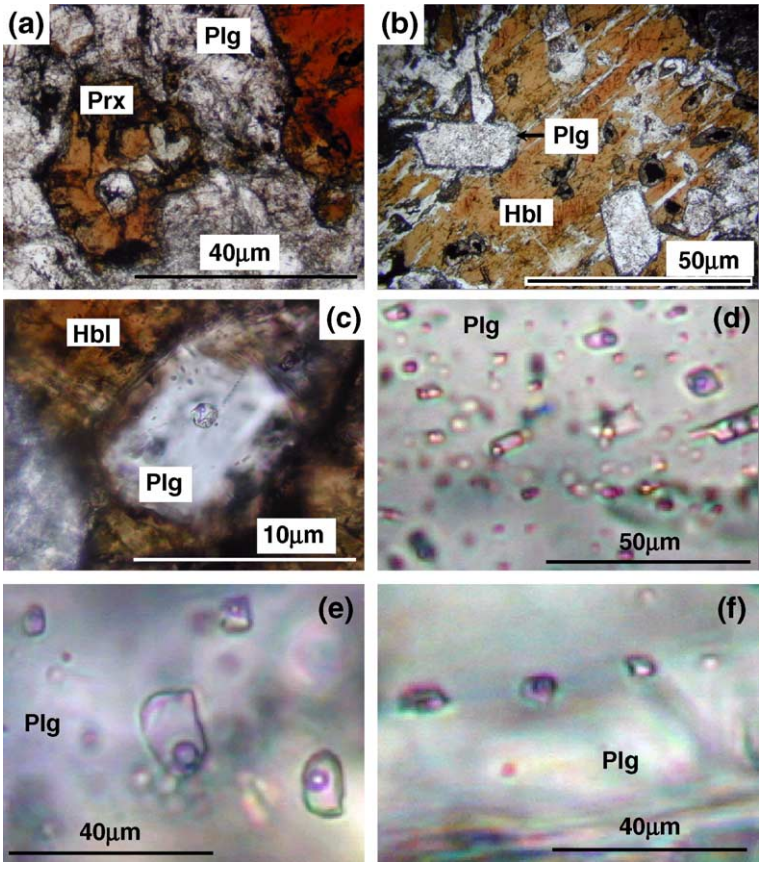

Fig. 3. Photomicrographs showing the petrographic feature and plagioclase-hosted fluid inclusions for the gabbro–norite from the central Xiangshan. (a) Subhedral pyroxene (Prx) coexists with plagioclase (Plg), showing a regular interface, Sample Xis4. (b) Poikilitic hornblende (Hbl) megacryst grows around plagioclase, Xis2. (c) A fluid inclusion is trapped within the plagioclase that is surrounded by hornblende, Xis4. (d) Fluid inclusions, varying in size, occur in group without obvious orientation, Xis2. (e) Isolated fluid inclusions show relatively large sizes, Xis2. (f) Fluid inclusion trail occurs parallel to the grain boundary of the host plagioclase, Xis1. All photomicrographs taken with the plain light.

likely have been trapped from the exsolved magmatic fluid, and, hence, also derive from the mantle reservoir as the primary fluid inclusions.

As shown in the inset D of Fig. 1, the Huangshandong is a composite lopolith, and intrudes the carbonaceous siltstone, slate, and limestone of the Late Carboniferous Gandun formation. The Huangshandong includes three intrusions. Intrusion I is hornblende gabbro and minor hornblende–olivine gabbro, whereas intrusion II is peridotite and gabbro–norite. Intrusion III is peridotite, and cuts intrusions I and II. The studied sample HE17-1 was collected in the tunnel from intrusion II peridotite. As shown in Fig. 2(c) and (d), the peridotite is composed of olivine (43–50%), pyroxene (15–25%), plagioclase (10–20%), and hornblende (12–25%). Olivine is fine-grained (0.25–1 mm). The studied fluid inclusions are confined within olivine grain, and occur parallel to the grain boundary (Fig. 2 (e)) or without obvious orientation (Fig. 2(f)). These fluid inclusions are pseudo-secondary or primary, and, hence, were trapped during or soon following crystallization of olivine [55].

5. Experimental procedure and analytical results

From thin sections of the studied samples, we selected those fluid inclusions that are about 10 to 30 μm in size and show a depth of less than 20 μm to the surface. Fifteen fluid inclusions from KD and HE17-1 each, and about 50 fluid inclusions from Xis1, Xis2, and

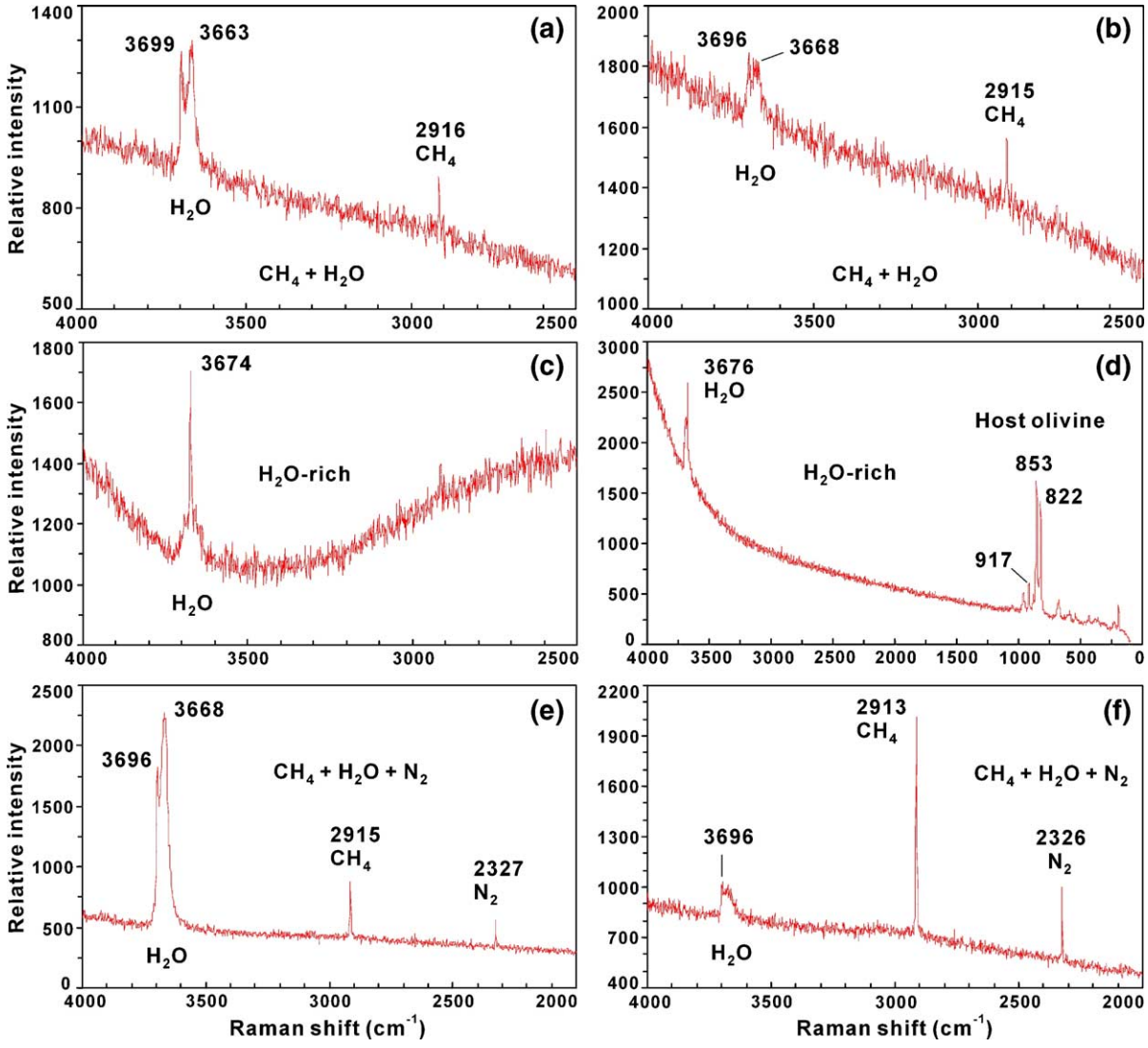

Fig. 4. Representative Raman spectra of olivine-hosted fluid inclusions from sample KD of the Kudi ophiolitic dunite.

Xis4 were analyzed using a Renishaw Raman MKI-1000 system equipped with a CCD detector and an Ar ion laser at the State Key Laboratory of Lithospheric Evolution, Institute of Geology and Geophysics, Chinese Academy of Sciences. The laser beam with a wavelength of 514.5 nm and a spot size of about 1 μm, was focused on the bubble and the surrounding liquid for each fluid inclusion through 50× and 100× objectives of a light microscope. The whole spectrum from 100 to 4000 cm^{-1} was scanned with a resolution of 2 cm^{-1}; the time of counting is 10 s for each wave number of 1 cm^{-1}. Representative Raman spectra for fluid inclusions from KD of the Kudi (Fig. 4), Xis1, Xis2, and Xis4 of the Xiangshan (Fig. 5), and HE17-1 of the Huangshandong (Fig. 6) are shown.

Raman spectrometric analyses of fluid inclusions in this study have resolved the major gaseous species from the 3 rock suites in the Xinjiang and yielded the relative intensity of Raman scatter for each species. These designate fluid types in the source region of the mantle and allow of an estimation of the relative abundances of the gaseous species. Olivine-hosted fluid inclusions from the Kudi dunite include 3 types of CH_4+H_2O (Fig. 4(a) and (b)), H_2O-rich (Fig. 4(c) and (d)), and $CH_4+H_2O+N_2$ (Fig. 4(e) and (f)). The abundance of CH_4 varies from below (Fig. 4(a) and (e)) to above (Fig. 4(f))

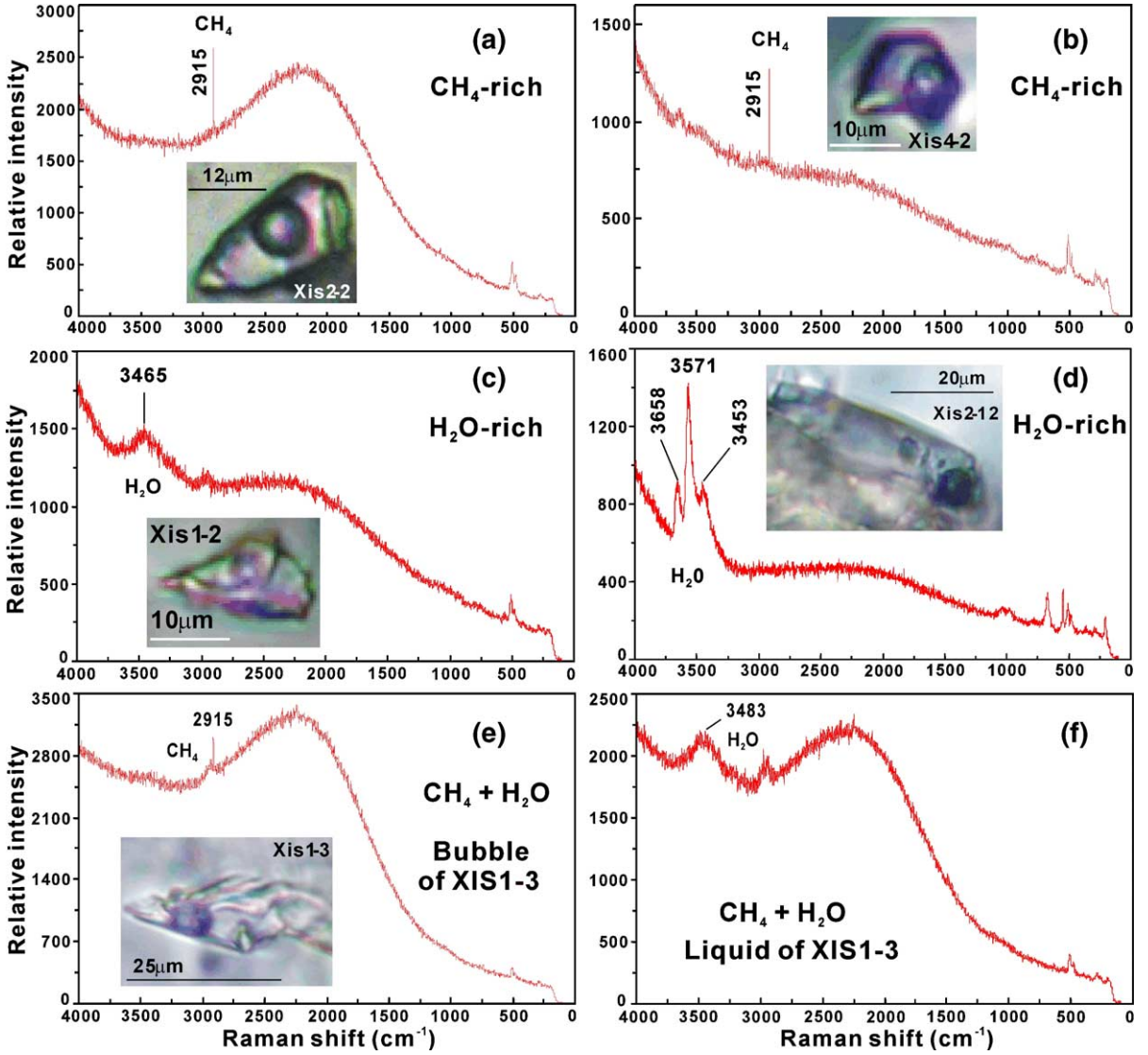

Fig. 5. Representative Raman spectra of plagioclase-hosted fluid inclusions from the gabbro–norite, central Xiangshan. Photomicrograph of the analyzed fluid inclusion is shown in each figure, with the sample name and the number of the fluid inclusion that has been analyzed specified.

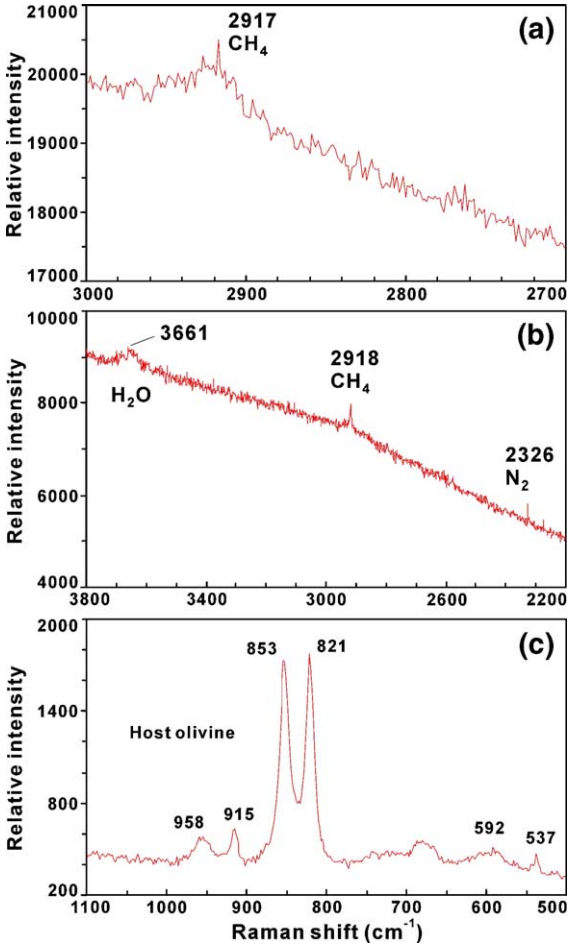

Fig. 6. Representative Raman spectra of olivine-hosted fluid inclusions ((a) and (b)) and the host olivine (c) from peridotite sample HE17-1, Huangshandong mafic–ultramafic intrusion.

that of H_2O, whereas the abundance of N_2 is variably lower than that of CH_4 (Fig. 4(e) and (f)). So, fluids brought from the mantle by the dunite of the Kudi ophiolite, western Kunlun Range, are CH_4–H_2O+N_2 type. Plagioclase-hosted fluid inclusions from the central Xiangshan gabbro–norite include CH_4-rich (Fig. 5(a) and (b)), H_2O-rich (Fig. 5(c) and (d)), and CH_4+H_2O (Fig. 5(e) and (f)), with notable absence of N_2. Olivine-hosted fluid inclusions from the Huangshandong peridotite are characterized by CH_4-rich (Fig. 6(a)) and CH_4+H_2O+N_2 (Fig. 6(b)) types. N_2, however, with a lower abundance than CH_4, is detected only in a few analyses. Therefore, fluids brought from the mantle by the post-collisional mafic–ultramafic intrusions of the central Xiangshan and the Huangshandong, eastern Chinese Tienshan Mts., are generally CH_4–H_2O type. In summary, fluids carried by these 3 rock suites from the Xinjiang are rich in reductive gaseous species CH_4 and H_2O plus minor N_2, with notable absence of CO_2.

6. Discussion

6.1. Estimation of the redox state, pressure and depth of formation for the melt–CH_4–H_2O+N_2 fluid systems from the 3 rock suites in the Xinjiang

Lithospheric upper mantle is relatively oxidized [56,57], with volatile components dominated by CO_2 [58,59]. CO_2-rich and CO_2–H_2O fluids equilibrate with diamond-free and diamond-bearing peridotites on the depths of less than 130 km or up to 200 km in the mantle, respectively, whereas CH_4–N_2-rich fluids equilibrate with metal–silicate melts on the depths of greater than 200 km in the much reduced asthenospheric mantle [60]. Computed equilibrium data also showed that a fluid with as much as 75% CH_4 can attain equilibrium with olivine in the deep mantle [61].

Graphite–C–O–H fluid equilibria in the crust conditions with pressures of less than 10 kbar have been studied by Frost [62], whereas Simakov [60] calculated pressure–temperature–oxygen fugacity (f_{O_2}) conditions and investigated fluid compositions for the peridotite–O–H–N–C fluid system under the upper mantle conditions. These approaches provide important means for us to estimate the degree of oxidation state, pressure and depth of formation for the melt–CH_4–H_2O+N_2 fluid systems from the 3 rock suites of the Xinjiang.

Volumetric percentages of the bubble and the liquid phases were measured along the macro- and the brachy-axes of fluid inclusions under the microscope. With assumption of pure CH_4 for the bubble phase, with neglect of N_2, and pure H_2O for the liquid phase, these volumetric percentages are converted into mole fractions of CH_4 and H_2O, i.e. X_{CH_4} and X_{H_2O}. At standard room conditions volatile components such as CH_4 and N_2, and H_2O tend to concentrate in the bubble and the liquid phases of fluid inclusions, respectively. In addition, CH_4-dominated bubble phases are commonly present in fluid inclusions from all the 3 rock suites (Figs. 4–6). So, the assumption for the mole fraction calculations is valid. From X_{CH_4}, f_{O_2} and pressure of formation for the melt–CH_4–H_2O+N_2 fluid systems from the 3 rock suites of the Xinjiang are estimated successively using the log (X_{CH_4}) vs. $-\log(f_{O_2})$ relationship (Fig. 7(a)) and the $\log(f_{O_2})-\log(QFM)$ vs. pressure relationship (Fig. 7(b)) of Simakov [60]. Ranges of these measured or estimated parameters for each of these 3 rock suites are summarized in Table 1. In

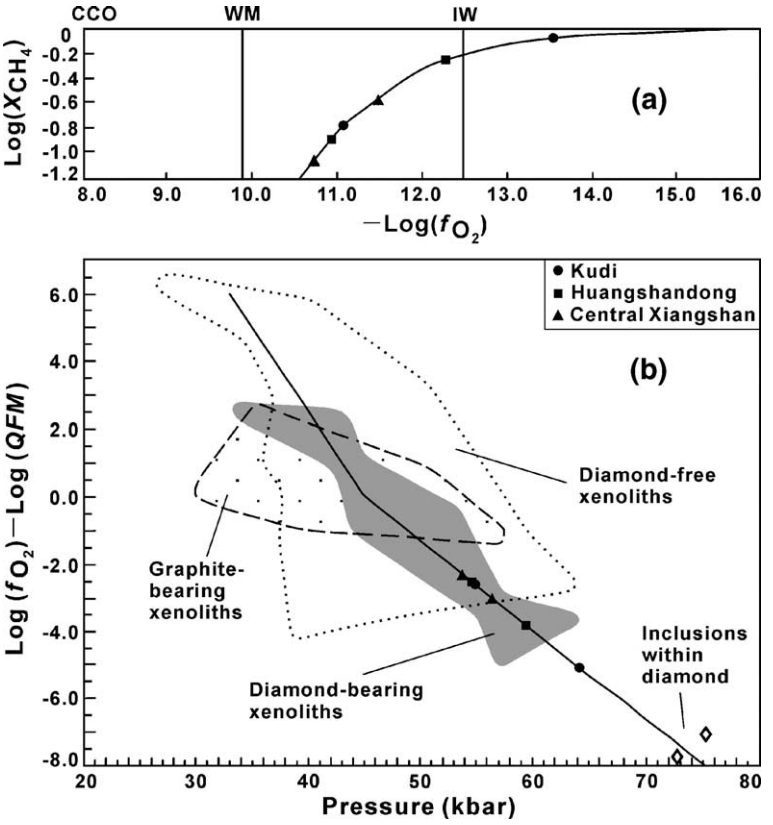

Fig. 7. (a) Estimation of the range of oxygen fugacity f_{O_2} for the CH_4–H_2O+N_2 fluids equilibrated with the 3 rock suites from the Xinjiang using the upper and the lower limit values of the estimated Log(X_{CH_4}) for the fluid inclusions, and the Log(X_{CH_4}) vs. −Log(f_{O_2}) relationship for the CH_4-dominated O–H–N–C gaseous system [60]. Oxygen buffers: CCO–CO_2(CO)–C–O_2; WM—wustite–magnetite, IW—iron–wustite. (b) Estimation of the range of formational pressures for the melt–CH_4–H_2O+N_2 fluid systems from the 3 rock suites of the Xinjiang using the upper and the lower limit values of the estimated f_{O_2} for these melt–fluid systems, and the dependence of Log(f_{O_2})−Log(QFM) on the pressure (kbar) for the mantle xenoliths and inclusions within diamond [60]. The fitted line to the xenoliths and inclusions within diamond defines the dependence.

conclusion, the CH_4–H_2O+N_2 fluids from these 3 rock suites of the Xinjiang have f_{O_2} varying from 10^{-11} to 10^{-14}; these upper and lower limit f_{O_2} values are ~1 log unit lower WM or IW buffer, respectively (Table 1 and Fig. 7(a)), hence suggesting a reduced source region in the upper mantle. The formational pressures for the 3 rock suites vary from 54 to 64 kbar, corresponding to depths from ~180 km to ~210 km (Table 1). As shown in Fig. 7(b), f_{O_2} values for the melt–CH_4–H_2O+N_2 fluid systems from the 3 rock suites of the Xinjiang are much lower than those for the diamond-free and the graphite-bearing mantle xenoliths, but vary from the low f_{O_2} domain for the diamond-bearing mantle xenoliths to beyond the latter towards the data of inclusions within diamonds. Zoned diamonds have recorded initial growth in equilibrium with the CH_4–N_2-rich fluid in the asthenosphere followed by subsequent growth and formation in equilibrium with the H_2O–CO_2 fluid near the boundary of lithosphere and asthenosphere [63]. However, such a transition for the formation of subcratonic mantle parageneses is not the cause for the generation of the melt–fluid systems from the 3 rock suites of the Xinjiang under the CAOB regime. Presence of abundant CH_4 and absence of CO_2 in those melt–fluid systems of the Xinjiang are much different from the H_2O–CO_2 fluid near the boundary of lithosphere and asthenosphere, while abundant H_2O in those systems are distinct from the CH_4–N_2-rich fluid in the much reduced asthenosphere.

Recent observation of converted seismic waves has shown that as much as 700 ppm of H_2O is present in the mantle transition zone at 400 km and greater depths [64]. Minerals in the deep mantle can contain a substantial amount of water: as much as 1000 ppm of H_2O in olivine and about 20,000 ppm of H_2O in wadsleyite [65]. Ultrahigh pressure metamorphic rocks as indicated by the coesite pseudomorphs in garnet and quartz exsolution lamellae in eclogitic omphacite,

Table 1
Ranges of the measured or estimated parameters for each of the 3 melt–fluid systems from the Kudi, the Huangshandong, and the central Xiangshan in the Xinjiang

Rock location	Sample lithology	Host mineral	Bubble (vol.%)	Liquid (vol.%)	X_{CH_4} [a]	X_{H_2O} [a]	Log (X_{CH_4})	Log (f_{O_2}) [b]	Log(f_{O_2}) − Log(QFM)	Formational pressure (kbar) [c]	Depth of formation (km) [d]
Kudi	Ophiolitic dunite	Olivine	0.2	0.8	0.17	0.83	−0.78	−11.1	−2.6	55	182
			0.85	0.15	0.82	0.18	−0.09	−13.6	−5.1	64	211
Huangshandong	Peridotite	Olivine	0.15	0.85	0.12	0.88	−0.90	−11	−2.5	55	182
			0.6	0.4	0.55	0.45	−0.26	−12.3	−3.8	59	195
Central Xiangshan	Gabbro–norite	Labrador	0.1	0.9	0.08	0.92	−1.08	−10.8	−2.3	54	178
			0.3	0.7	0.26	0.74	−0.59	−11.5	−3.0	56	185

[a] With the assumption of pure CH_4 for the bubble phase and pure H_2O for the liquid phase, the mole fractions of CH_4 (X_{CH_4}) and H_2O (X_{H_2O}) are calculated from the volumetric percentages of the bubble and the liquid phases of fluid inclusions using the densities at standard conditions for CH_4 gas (0.717 g/l) and liquid H_2O (1) and their molecular masses, respectively.
[b] Oxygen fugacity f_{O_2} in common logarithm is estimated graphically in the Log(X_{CH_4}) vs. −Log(f_{O_2}) diagram (Fig. 7(a)).
[c] The formational pressure is estimated graphically in the Log(f_{O_2}) − Log(QFM) vs. pressure diagram (Fig. 7(b)), with $f_{O_2}=10^{-8.5}$ for the oxygen buffer of quartz–fayalite–magnetite (QFM) [84].
[d] Depth of formation is obtained from the formational pressure multiplied by 33 km/10 kbar.

western Chinese Tienshan Mts. [66,67] suggest deep subduction of oceanic slab; eclogitic–facies veins and abundant primary aqueous fluid inclusions hosted by omphacite in the same belt provide direct evidence for the transfer of H_2O to the deep mantle together with the meta-subduction complex [68]. Ultrahigh pressure metamorphic belt in the western Chinese Tienshan Mts. extends westwards to the Atabishi blueschist–eclogite belt, Kirghizia [69,70], Fan–Karategin blueschist belt, Tajikistan [71], and the Kokchetav massif, Kazakhstan [72], and eastwards to the Kumishi blueschist belt [73]. Deep subduction of hydrated, oxidized ocean-floor before the terminal Early Carboniferous has brought abundant H_2O to the deep mantle, which accounts for the abundant inclusion H_2O from the 3 rock suites of the Xinjiang. Meanwhile, the presence of H_2O-rich fluid in the deep mantle underneath the Palaeo-Asian Ocean provides another line of evidence for the deep subduction of oceanic slab in the Xinjiang.

N_2 was known as one of the main gaseous species in the kimberlite breccias (e.g. [74]), the olivine glasses from lamproite [75], and the ocean-floor basalts [76]. Nitrogen is the main structural admixture in natural diamonds [77] and can reach about 70–90% by volume in gaseous inclusions from diamonds [78]. Decrease of nitrogen concentration is due to its dissolution into the mafic and ultramafic melts [79] by the reaction:

$$Mg_2SiO_4 + 3C + N_2 \rightarrow MgO + MgSiN_2 + 3CO.$$

Oxidation of carbon and melting in the mantle facilitate the nitrogen dissolution. So, inclusion N_2 from the 3 rock suites of the Xinjiang is residual from the primordial mantle fluids after dissolution into the melts.

As introduction of significant amounts of H_2O into the deep mantle has variably diluted CH_4, the afore-estimated X_{CH_4} and, hence, pressure and depth are underestimates, whereas f_{O_2} is overestimate. Before slab subduction, fluids from the deep mantle underneath the Xinjiang likely are CH_4–N_2 type. These CH_4–N_2 fluids are stable at much reduced asthenospheric mantle, with depth greater than 200 km and f_{O_2} in the region of IW buffer, where inclusions within the diamond are formed [60].

In conclusion, fluids carried by the ophiolitic dunite and post-collisional mafic–ultramafic intrusions in the Xinjiang have derived from the asthenospheric mantle underneath the Palaeo-Asian Ocean through to the post-collisional period. Originally, these fluids were CH_4–N_2 type and were primordial mantle fluid. Subduction of oceanic slab and resultant introduction of H_2O into the deep mantle, and dissolution of N_2 into the melts changed this CH_4–N_2-type fluid into the fluid of CH_4–H_2O plus minor N_2 as presently preserved in these 3 rock suites.

6.2. Protracted redox melting in the mantle underneath the Palaeo-Asian Ocean through to the post-collisional period

The prevalence of CH_4–H_2O-rich fluid in the deep mantle underneath the Palaeo-Asian Ocean through to the post-collisional period has important implications for the mantle dynamics. Taylor and Green [80] experimentally showed that initial melting of peridotite saturated with H_2O–CH_4 fluids occurs at temperatures

well above stable continental geotherms. This implies that C–H–O fluid-induced melting in the mantle will be restricted to regions where the CH_4-rich fluid undergoes sufficient oxidation or dilution with H_2O by interaction with oxidized, hydrated lithosphere (redox melting), or where the geotherm is abnormally high (hot-spot melting), or where there is some combination of these processes.

Occurrence of micro-inclusions of brine, carbonates and silicate minerals within cloudy diamonds suggests that such brine and carbonates are important for mantle melting and diamond growth in both eclogitic and peridotitic environments [81]. The seawater-derived brines have been brought to the stability field of diamond in the mantle by subducted marine sediments and altered basalt [81]. Oxidation of C–H–O fluids either by introduction of carbonate and oxygen impurities or by dilution with H_2O promotes mantle melting and diamond growth [81–83].

As shown in Table 1 and Figs. 4–7, X_{CH_4} and the relative abundance of N_2 tend to decrease, but X_{H_2O} and f_{O_2} increase from the melt–CH_4–H_2O+N_2 fluid system for the Kudi ophiolitic dunite, western Kunlun Range, to the melt–CH_4–H_2O fluid systems for the post-collisional mafic–ultramafic intrusions of the Huangshandong and the central Xiangshan, eastern Chinese Tienshan Mts. This variation from before to after the final closure of the Palaeo-Asian Ocean, although for a relatively short time segment during the prolonged evolution of this ocean, has nevertheless recorded the progressive oxidation and dilution of the primordial mantle fluid. Subduction of oceanic slab from terminal Mid-Proterozoic through to the Late Paleozoic incessantly but heterogeneously oxidized and hydrated the mantle underneath the Palaeo-Asian Ocean. This promoted repeated redox melting in the mantle and, hence, caused formation of the long-lived Palaeo-Asian Ocean with repeated open–closing processes and its westward migration. The redox melting in the mantle continued through to the post-collisional period after the final closure of the Palaeo-Asian Ocean, brought about extensive intrusion of mafic–ultramafic complexes and alkaline–peralkaline granites in or near the former suture zone where abundant oceanic materials were available to the underlying deep mantle, induced widespread hydrothermal–mineralization, and, consequently, resulted in significant continental growth in the Central Asian Orogenic Belt. Furthermore, occurrence of adakite and related igneous rocks in the Xinjiang implies that high-temperature melting also has played a role in the mantle dynamics underneath the Palaeo-Asian Ocean through to the post-collisional period.

6.3. Mantle redox evolution and continental growth

Mantle redox evolution is intimately linked to the oxidation state of the primitive atmosphere. The upper mantle was originally more reduced than today, and has become progressively more oxidized as a consequence of the release of reduced volcanic gases and the subduction of hydrated, oxidized ocean-floor [84]. Gases released from natural diamonds include H_2O, H_2, CO_2, CH_4, N_2, CO, etc. [78,85]. Micro-inclusions of brine and carbonates occur in cloudy diamonds [81]. These results show the presence of abundant CO_2 and CO besides H_2O in the mantle and, hence, suggest an oxidizing nature for the mantle fluids. CH_4-mediated H escape to space orders of magnitude faster than today irreversibly oxidizes the Earth [57]. The major oxidation of the Earth and the rise of atmospheric O_2 occurred at about 2.4 to 2.2 Ga [86–90]. Currently, Earth gains oxygen by CH_4-induced H escape at a negligible rate [57].

On the other hand, the Earth's continents have grown after 2.5 Ga, with minor additions in the Phanerozoic times [91–94]. The two fundamental processes of the Earth's oxidation and formation of bulk of the continent are temporally broadly coupled. We infer that oxidation of the Earth's mantle has efficiently reduced the CH_4 content and, thus, promoted the mantle melting and magma input to the crust, resulting in major continental growth after 2.5 Ga broadly concurrent with the major oxidation of the Earth.

The characteristics of high $\varepsilon_{Nd}(t)$, low initial $(^{87}Sr/^{86}Sr)_t$ values are not unique to Phanerozoic granitoids in the Central Asian Orogenic Belt, but are shared by Phanerozoic granitoids in areas such as the New England and the Lachlan Belts, southeastern Australia (e.g. [95–98]), the Cordillera of North America (e.g. [99–101]), Newfoundland Appalachians, Canada (e.g. [102]), and the Africa (e.g. [103]). The fayalite or high-silica rhyolites in the Yellowstone–Snake River Plain province (e.g. [104]) and the Basin and Range province (e.g. [105]), USA, show similar characteristics. Granitoids and the rhyolites in these areas suggest significant continental growth during the Phanerozoic times via basaltic underplating and re-melting of the newly underplated materials [45,106]. Meanwhile, abundance of the CH_4-rich fluid inclusions in the Paleozoic ophiolitic dunite and the mafic–ultramafic intrusions in the Xinjiang, China, reveals preservation of the reduced primordial mantle underneath the Palaeo-Asian Ocean through to the Late Paleozoic time. Postponed oxidation of the reduced primordial mantle underneath the Central Asian Orogenic Belt led to

mantle melting and significant continental growth in the Phanerozoic times that, too, is much postponed compared with the major continental growth during the late Archaean times. At present, the redox evolution of the mantle underneath the aforementioned areas in the world showing significant Phanerozoic continental growth is unknown yet, so we are uncertain that to what extent these two fundamental processes of mantle redox melting and continental growth are globally linked. In any case, the current models regarding the redox evolution of the Earth's mantle and the continental growth should take the above facts into serious account.

7. Conclusions

The Kudi ophiolite (Late Cambrian–earliest Ordovician), western Kunlun Range, represents the southernmost portion of the Palaeo-Asian Ocean. The central Xiangshan (285 Ma) and the Huangshandong (282–274 Ma) intrusions are typical of the post-collisional mafic–ultramafic complexes of the Xinjiang. Olivine- and plagioclase-hosted fluid inclusions from the Kudi ophiolitic dunite, the central Xiangshan and the Huangshandong intrusions are rich in H_2O and CH_4 with variable amounts of N_2. These fluids have derived from the reduced asthenospheric mantle underneath the Palaeo-Asian Ocean through to the post-collisional period. These fluids were originally CH_4–N_2-rich, primordial mantle fluid, but were progressively oxidized and diluted with H_2O by long-term subduction of the oceanic slab. Repeated redox melting in the mantle generated the long-lived Palaeo-Asian Ocean, caused extensive intrusion of mafic–ultramafic complexes and alkaline–peralkaline granites through to the post-collisional period, and, consequently, resulted in significant continental growth in the Central Asian Orogenic Belt. Major oxidation of the Earth's mantle at about 2.4 to 2.2 Ga promoted the mantle melting, hence resulting in major continental growth after 2.5 Ga. However, much-postponed oxidation of the primordial mantle underneath the Central Asian Orogenic Belt postponed significant continental growth until the Phanerozoic times. Future work should be focused on the redox evolution of the mantle underneath such areas in the world that show significant Phanerozoic continental growth, in order to link these two fundamental processes of mantle redox melting and the continental growth.

Acknowledgements

The authors would like to express our thanks to an anonymous reviewer for constructive comments. Dr. W.-J. Xiao, Prof. X.-C. Xiao, Dr. J.-Y. Li, Dr. J. Gao, and Dr. Y.-T. Wang are acknowledged for helpful discussions. This study was granted by the Ministry of Science and Technology of China (No. 2001CB409803) and the National Science Foundation of China (No. 40472056).

References

[1] P.K. Kepezhinskas, K.B. Kepezhinskas, I.S. Pukhtel, Lower Paleozoic oceanic crust in Mongolian Caledonides: Sm–Nd isotope and trace element data, Geophys. Res. Lett. 18 (1991) 1301–1304.

[2] Y.V. Amelin, L.A. Neymark, E.Y. Ritsk, A.A. Nemchin, Enriched Nd–Sr–Pb isotopic signatures in the Dovyren layered intrusion (eastern Siberia, Russia): evidence for source contamination by ancient upper-crustal material, Chem. Geol. 129 (1996) 39–69.

[3] Y.V. Amelin, E.Y. Ritsk, L.A. Neymark, Effects of interaction between ultramafic tectonite and mafic magma on Nd–Pb–Sr isotopic systems in the Neoproterozoic Chaya Massif, Baikal–Muya ophiolite belt, Earth Planet. Sci. Lett. 148 (1997) 299–316.

[4] V.E. Khain, G.S. Gusev, E.V. Khain, V.A. Vernikovsky, M.I. Volobuyev, Circum-Siberian Neoproterozoic ophiolite belt, Ofioliti 22 (1997) 195–200.

[5] J.A. Pfänder, K.-P. Jochum, A. Kröner, I. Kozakov, C. Oidup, W. Todt, Age and geochemical evolution of an Early Cambrian ophiolite-island arc system in Tuva, south Central Asia, Geol. Surv. Finland Spec. Paper, vol. 26, 1998, p. 42.

[6] A.S. Gibsher, E.V. Khain, A.B. Kotov, E.B. Salnikova, I.K. Kozakov, V.P. Kovach, S.Z. Yakovleva, A.M. Fedoseenko, Late Vendian age of Khan–Taishiri ophiolite complex in western Mongolia, Russ. Geol. Geophys. 42 (2001) 1171–1177.

[7] O.M. Turkina, Tonalite–trondhjemite of subduction-related complexes (Late Riphean plagiogranites) on the SW margin of the Siberian craton, Russ. Geol. Geophys. 43 (2002) 418–431.

[8] E.V. Khain, E.V. Bibikova, A. Kröner, D.Z. Zhuravlev, E.V. Sklyarov, A.A. Fedotova, I.R. Kravchenko-Berezhnoy, The most ancient ophiolite of the Central Asian fold belt: U–Pb and Pb–Pb zircon ages for the Dunzhugur Complex, Eastern Sayan, Siberia, and geodynamic implications, Earth Planet. Sci. Lett. 199 (2002) 311–325.

[9] A.A. Mossakovskii, S.V. Ruzhentsev, S.G. Samygin, T.N. Kheraskova, Central Asian fold belt: geodynamic evolution and history of formation, Geotectonics 6 (1993) 3–33.

[10] E.V. Khain, E.V. Bibikova, E.B. Salnikova, A. Kröner, A.S. Gibsher, A.N. Didenko, K.E. Degtyarev, A.A. Fedotova, The Palaeo-Asian ocean in the Neoproterozoic and early Paleozoic: new geochronological data and palaeotectonic reconstruction, Precambrian Res. 122 (2003) 329–358.

[11] X.-C. Xiao, Y.-Q. Tang, J.-Y. Li, M. Zhao, Y.-M. Feng, B.-Q. Zhu, On the tectonic evolution of the southern margin of the Paleozoic composite megasuture zone, in: X.-C. Xiao, Y.-Q. Tang (Eds.), On the Tectonic Evolution of the Southern Margin of the Paleozoic Composite Megasuture Zone, Beijing Science and Technological Press, Beijing, 1991, pp. 1–29 (in Chinese with English abstract).

[12] S. Gurschka, A. Kröner, A.V. Avdeev, N.S. Seitov, R. Oberhänsli, Early Paleozoic accretion of arcs and microcontinents in the

Central Asian Mobile Belt of southern Kazakhstan as deduced from Pb–Pb zircon and Sm–Nd model ages, Terra Nova 9 (1997) (Abstr.—Suppl. 1, 340).
[13] XBGMR, Memoir of Xinjiang Geology, Xinjiang Bureau of Geological Mineral and Resource, Geological Publishing House, Beijing, 1993.
[14] W.-J. Xiao, B.F. Windley, J. Hao, J.-L. Li, Arc–ophiolite obduction in the Western Kunlun Range (China): implications for the Paleozoic evolution of central Asia, J. Geol. Soc. (Lond.) 159 (2002) 517–528.
[15] S.T. Kwon, G.R. Tilton, R.G. Coleman, Y. Feng, Isotopic studies bearing on the tectonics of the west Junggar region, Xinjiang, China, Tectonics 8 (1989) 719–727.
[16] Y. Feng, R.G. Coleman, G.R. Tilton, X. Xiao, Tectonic evolution of the west Junggar region, Xinjiang, China, Tectonics 8 (1989) 729–752.
[17] W. Liu, Whole rock isochron ages of plutons, crustal movements and evolution of tectonic setting in the Altay Mts. Xinjiang Uygur Autonomous Region, Geoscience of Xinjiang, vol. 4, Geological Publishing House, Beijing, 1993, pp. 35–50 (in Chinese with English abstract).
[18] W.-J. Xiao, B.F. Windley, Q.-R. Yan, K.-Z. Qin, H.-L. Chen, C. Yuan, M. Sun, J.-L. Li, S. Sun, SHRIMP zircon age of the Aermantai ophiolite in the North Xinjiang, China and its tectonic implications, Acta Geologica Sinica 80 (in press) (in Chinese with English abstract).
[19] J.-Y. Li, On the evolution of the Paleozoic plate tectonics of the east Junggar, Xinjiang, China, in: X.C. Xiao, Y.Q. Tang (Eds.), Tectonic Evolution of the Southern Margin of the Paleo-Asian Composite Megasuture, Beijing Science and Technological Press, Beijing, 1991, pp. 92–108 (in Chinese with English abstract).
[20] C. Zhang, X. Huang, M.-G. Zhai, Geological characteristics of the ophiolites, and their tectonic settings and ages, western Junggar, Xinjiang, Bull. Inst. Geol. Chin. Acad. Sci., Sci. Press, Beijing, 1995, pp. 165–218 (in Chinese).
[21] J.-Y. Li, Main characteristics and emplacement processes of the east Junggar ophiolites, Xinjiang, China, Acta Petrol. Sin. 11 (1995) 73–84 (Supp.) (in Chinese with English abstract).
[22] Z.-F. Chen, S.-D. Chen, Y.-H. Liang, Opening–Closing Tectonics of Xinjiang and Mineralization, Xinjiang Technological and Sanitation Press, Urumqi, 1997 (in Chinese with English abstract).
[23] Z.-H. Wang, S. Sun, J.-L. Li, Q.-L. Hou, K.-Z. Qin, W.-J. Xiao, J. Hao, Paleozoic tectonic evolution of the northern Xinjiang, China: geochemical and geochronological constraints from the ophiolites, Tectonics 22 (2) (2003) 1014, doi:10.1029/2002TC001396.
[24] S.-S. Sun, W.F. McDonough, Chemical and isotopic systematics of oceanic basalts: implications for mantle composition and processes, in: A.D. Saunders, M.J. Norry (Eds.), Magmatism in the Ocean Basins, Geol. Soc. Spec. Publ., vol. 42, 1989, pp. 313–345.
[25] Q. Wang, Z.-H. Zhao, Z.-H. Bai, Z.-W. Bao, J.-F. Xu, X.-L. Xiong, H.-J. Mei, Y.-X. Wang, Carboniferous adakites and Nb-enriched arc basaltic rocks association in the Alataw Mountains, northern Xinjiang: interactions between slab melt and mantle peridotite and implications for crustal growth, Chin. Sci. Bull. 48 (19) (2003) 2108–2115.
[26] J.-F. Xu, H.-J. Mei, X.-Y. Yu, Z.-H. Bai, H.-C. Liu, F.-R. Chen, Z.-P. Zheng, Q. Wang, Late Paleozoic subduction-related adakites in the northern margin of Junggar: partial melting products of subducting slab, Chin. Sci. Bull. 46 (2001) 684–688.
[27] M.J. Defant, M.S. Drummond, Derivation of some modern arc magmas by melting of young subducted lithosphere, Nature 347 (1990) 662–665.
[28] M.B. Allen, B.F. Windley, C. Zhang, Paleozoic collisional tectonics and magmatism of the Chinese Tien Shan, central Asia, Tectonophysics 220 (1992) 89–115.
[29] E. Sobel, N. Arnaud, A possible middle Paleozoic suture in the Altyn Tagh, NW China, Tectonics 18 (1999) 64–74.
[30] Z. He, S. Tian, Z. Xu, J. Yang, J. Cui, Discovery of the Late Paleozoic radiolarian fossils in the middle segment of the Altyn Tagh and its implication, Sci. Geol. Sin. 45 (1999) 246.
[31] C. Yuan, Magmatism and tectonic evolution of the West Kunlun Mountains, PhD dissertation, University of Hong Kong, 1999.
[32] H.-Q. Li, C.-F. Xie, H.-L. Chang, H. Cai, J. Zhu, S. Zhou, Study on Metallogenetic Chronology of Nonferrous and Precious Metallic Ore Deposits in North Xinjiang, China, Geological Publishing House, Beijing, 1998, pp. 1–264 (in Chinese with English abstract).
[33] B.-F. Han, J.-Q. Ji, B. Song, L.-H. Chen, Z.-H. Li, SHRIMP zircon U–Pb ages of Kalatongke No. 1 and Huangshandong Cu–Ni-bearing mafic–ultramafic complexes, North Xinjiang, and geological implications, Chin. Sci. Bull. 49 (2004) 2424–2429.
[34] J.-W. Mao, J.-M. Yang, W.-J. Qu, et al., Re–Os ages of Cu–Ni ores from the Huangshandong Cu–Ni sulfide deposit in the East Tianshan Mountains and its implications for geodynamic process, Acta Geol. Sin. 77 (2) (2003) 220–226.
[35] K.-Z. Qin, L.-C. Zhang, W.-J. Xiao, et al., Overview of major Au, Cu, Ni and Fe deposits and metallogenic evolution of the eastern Tianshan Mountains, Northwestern China, in: J.-W. Mao, R.J. Goldfarb, R. Seltmann, et al., (Eds.), Tectonic Evolution and Metallogeny of the Chinese Altai and Tianshan, London, CERCAMS/NHM, IAGOD Guidebook Series, vol. 10, 2003, pp. 227–248.
[36] W. Liu, Quantitative modeling of source rocks for granitoids in the Altai Mts., Xinjiang Uygur Autonomous Region, China, Geotecton. Metallogen. 15 (3) (1991) 199–208 (in Chinese with English abstract).
[37] C.-S. Bi, X.-Y. Shen, Q.-S. Xu, Isotope geology of the Beilekuduke tin metallogenic belt in Xinjiang, Geoscience of Xinjiang, vol. 5, Geological Publishing House, Beijing, 1994, pp. 106–119 (in Chinese with English abstract).
[38] L.-X. Gu, Q. Zhu, S.-X. Hu, et al., Geological characteristics and origin of the Kelameili–Harlik alkali granite belt, Xinjiang, Geoscience of Xinjiang, vol. 2, Geological Publishing House, Beijing, 1994, pp. 47–55 (in Chinese with English abstract).
[39] Q.-X. Lu, X.-F. Liu, Isotope geochemical studies on tin-bearing granite rock belt in west part of eastern Junggar, Xinjiang, Geoscience of Xinjiang, vol. 5, Geological Publishing House, Beijing, 1994, pp. 132–143 (in Chinese with English abstract).
[40] B.-F. Han, S.-G. Wang, B.-M. Jahn, et al., Depleted-mantle source for the Ulungur River A-type granites from North Xinjiang, China: geochemistry and Nd–Sr isotopic evidence, and implications for Phanerozoic crustal growth, Chem. Geol. 138 (3–4) (1997) 135–159.
[41] G.-H. Sun, J.-Y. Li, L.-M. Gao, T.-N. Yang, Zircon SHRIMP U–Pb age of a dioritic pluton in the Haerlike Mountain, eastern Xinjiang, and its tectonic implication, Geol. Rev. 51 (4) (2005) 463–469 (in Chinese with English abstract).

[42] A.N. Zanvilevich, B.A. Litvinovsky, S.M. Wickham, F. Bea, Genesis of alkaline and peralkaline syenite–granite series: the Kharitonovo pluton (Transbaikalia Russia), J. Geol. 103 (1995) 127–145.
[43] V.I. Kovalenko, V.V. Yarmolyuk, V.P. Kovach, A.B. Kotov, I.K. Kozakov, E.B. Sal'nikova, Sources of Phanerozoic granitoids in Central Asia: Sm–Nd isotope data, Geochem. Int. 34 (1996) 628–640.
[44] B.M. Jahn, F. Wu, B. Chen, Massive granitoid generation in Central Asia: Nd isotopic evidence and implication for continental growth in the Phanerozoic, Episodes 23 (2000) 82–92.
[45] L. Wei, W. Siebel, X.-J. Li, X.-F. Pan, Petrogenesis of the Linxi granitoids, northern Inner Mongolia of China: constraints on basaltic underplating, Chem. Geol. 219 (2005) 5–35.
[46] X.-L. Xiong, Z.-H. Zhao, Adakite-type sodium-rich rocks in Awulale Mountains of the western Tianshan: significance for the vertical growth of continental crust, Chin. Sci. Bull. 46 (7) (2001) 811–817.
[47] S.-H. Yan, W. Chen, Y.-T. Wang, $^{40}Ar/^{39}Ar$ ages of the Erqisi gold metallogenetic belt, Xinjiang, and their geological significance, Acta Geol. Sin. 78 (4) (2004) 500–506 (in Chinese with English abstract).
[48] Z.-Y. Rui, R.J. Goldfarb, Y.-M. Qiu, T.-H. Zhou, R.-Y. Chen, F. Pirajno, G. Yun, Paleozoic–early Mesozoic gold deposits of the Xinjiang Autonomous Region, northwestern China, Miner. Depos. 37 (2002) 393–418.
[49] W. Liu, X.-J. Li, J. Deng, Sources of ore-forming fluids and metallic materials in the Jinwozi lode gold deposit, eastern Tianshan Mountains of China, Sci. China, Ser. D 46 (2003) 137–153 (Supp.).
[50] Z.-L. Wang, N. Jiang, Y.-T. Wang, et al., Genesis of the Kanggur gold deposit in the eastern Tianshan orogenic belt, NW China: fluid inclusion and oxygen and hydrogen isotope constraints, Resour. Geol. 54 (2) (2004) 177–185.
[51] F.-Q. Yang, Y.-T. Wang, et al., The Bulong gold deposit—a quartz–barite vein type gold deposit in the Xinjiang: geological characteristics and S, He and Ar isotopic compositions, Acta Geol. Sin. 78 (2) (2004) 404–416.
[52] P.H. Matte, P. Tapponnier, N. Arnaud, et al., Tectonics of western Tibet, between the Tarim and the Indus, Earth Planet. Sci. Lett. 142 (1996) 311–330.
[53] F. Mattern, W. Schneider, Suturing of the Proto- and Paleo-Tethys oceans in the western Kunlun (Xinjiang, China), J. Asian Earth Sci. 18 (2000) 637–650.
[54] Z.-H. Wang, S. Sun, Q.-L. Hou, J.-L. Li, Effect of melt–rock interaction on geochemistry in the Kudi ophiolite (western Kunlun Mountains, northwestern China): implication for ophiolite origin, Earth Planet. Sci. Lett. 191 (2001) 33–48.
[55] E. Roedder, Fluid inclusions, Rev. Miner. 12 (1984) 250–290.
[56] C. Lécuyer, Y. Ricard, Long-term fluxes and budget of ferric iron: implication for the redox states of the Earth's mantle and atmosphere, Earth Planet. Sci. Lett. 165 (1999) 197–211.
[57] D.C. Catling, K.J. Zahnle, C.P. McKay, Biogenic methane, hydrogen escape, and the irreversible oxidation of early Earth, Science 293 (2001) 839–843.
[58] W.F. Giggenbach, The origin and evolution of fluids in magmatic–hydrothermal systems, in: H.L. Barnes (Ed.), Geochemistry of Hydrothermal Ore Deposits, 3rd ed., Wiley, New York, 1997, pp. 737–796.
[59] J.B. Lowenstern, Carbon dioxide in magmas and implications for hydrothermal systems, Miner. Depos. 36 (2001) 490–502.
[60] S.K. Simakov, Redox state of Earth's upper mantle peridotites under the ancient cratons and its connection with diamond genesis, Geochim. Cosmochim. Acta 62 (10) (1998) 1811–1820.
[61] S.K. Saxena, Oxidation state of the mantle, Geochim. Cosmochim. Acta 53 (1989) 89–95.
[62] B.R. Frost, Mineral equilibria involving mixed-volatiles in a C–O–H fluid phase: the stabilities of graphite and siderite, Am. J. Sci. 279 (1979) 1033–1059.
[63] V.K. Garanin, G.P. Kudryavtseva, Morphology, physical properties and paragenesis of inclusion-bearing diamonds from Yakutian kimberlites, Lithos 25 (1990) 211–217.
[64] M. van der Meijde, F. Marone, D. Giardini, S. van der Lee, Seismic evidence for water deep in Earth's upper mantle, Science 300 (2003) 1556–1558.
[65] D. Kohlstedt, H. Keppler, D. Rubie, Solubility of water in the α, β and γ phases of $(Mg,Fe)_2SiO_4$, Contrib. Mineral. Petrol. 123 (1996) 345–357.
[66] L. Zhang, D.J. Ellis, W. Jiang, Ultrahigh-pressure metamorphism in the western Tianshan, China: Part I. Evidence from inclusions of coesite pseudomorphs in garnet and from quartz exsolution lamellae in omphacite in eclogite, Am. Mineral. 87 (2002) 853–860.
[67] L. Zhang, D.J. Ellis, W. Jiang, Ultrahigh-pressure metamorphism in the western Tianshan, China: Part II. Evidence from inclusions of coesite pseudomorphs in garnet and from quartz exsolution lamellae in omphacite in eclogite, Am. Mineral. 87 (2002) 860–866.
[68] J. Gao, R. Klemd, Primary fluids entrapped at blueschist to eclogite transition: evidence from the Tianshan meta-subduction complex in northwestern China, Contrib. Mineral. Petrol. 142 (2001) 1–14.
[69] N.V. Sobolev, N.L. Dobretsov, L.B. Bakirov, V.S. Shatsky, Eclogites from various types of metamorphic complexes in the USSR and the problems of their origin, in: B.W. Evans, E.H. Brown (Eds.), Blueschists and Eclogites, Geol. Soc. Am. Mem., vol. 164, 1986, pp. 349–363.
[70] M. Tagiri, Y. Yano, A. Bakirov, T. Nakajima, S. Uchiumi, Mineral parageneses and metamorphic P–T paths of ultrahigh-pressure eclogites from Kyrghyzstan Tien-Shan, Isl. Arc 4 (1995) 280–292.
[71] N.I. Volkova, V.I. Budanov, Geochemical discrimination of metabasalt rocks of the Fan-Karategin transitional blueschist/greenschist belt, South Tienshan, Tajikistan: seamount volcanism and accretionary tectonics, Lithos 47 (1999) 210–216.
[72] I. Katayama, C.R. Parkinson, K. Okamoto, Y. Nakajima, S. Maruyama, Supersilicic clinopyroxene and silica exsolution in UHPM eclogite and pelitic gneiss from the Kokchetav Massif, Kazakhstan, Am. Mineral. 85 (2000) 1368–1374.
[73] J. Gao, X.-C. Xiao, Y.-Q. Tang, M. Zhao, J. Wang, H.-Q. Wu, The discovery of blueschist in Kumux of the southern Chinese Tienshan Mts., and its tectonic significance, Reg. Geol. China 4 (1993) 344–347 (in Chinese with English abstract).
[74] V. Gogini, C.E. Melton, A.A. Giardiny, Some petrological aspects of the Prairie Creek diamond-bearing kimberlite diatreme, Arkansas, Contrib. Mineral. Petrol. 66 (1978) 251–262.
[75] A.V. Sobolev, N.V. Sobolev, C.B. Smith, J. Dubessy, Fluid and melt compositions in lamproites and kimberlites based on the study of inclusions in olivine, in: J.R. Ross (Ed.), Kimberlites and Related Rocks, Proc. 4th Intl. Kimber. Conf., Spec. Publ. Geol. Soc. Aust., vol. 14, 1989, pp. 220–242.

[76] E.F. Shnikov, V.A. Kaluzhny, A.S. Shiritsa, L.F. Telenko, A.S. Kruglov, I.M. Svoren, Gaseous fluids of contact basalts from Indian ocean floor (from relict inclusions), Dokl. Akad. Nauk SSSR 297 (1987) 1457–1460 (in Russian).
[77] W. Kaiser, W.L. Bond, Nitrogen—a major impurity in common type 1 diamond, Phys. Rev. 115 (1959) 857–863.
[78] A.A. Giardini, C.E. Melton, Gases released from natural and synthetic diamonds by crushing under high vacuum at 200 °C, and their significance to diamond genesis, Fortschr. Mineral. Spec. Iss., vol. 52, 1975, pp. 455–464.
[79] A.N. Strehletov, G.U. Shvedenkov, N.U. Osorgin, T.K. Kazimirova, Nitrogen solubility in the melts of the system $CaO–MgO–Al_2O_3–SiO_2$, Geol. Geofiz. 31 (1990) 81–85 (in Russian).
[80] W.R. Taylor, D.H. Green, Measurement of reduced peridotite–C–O–H solidus and implications for redox melting of the mantle, Nature 332 (1988) 349–352.
[81] E.S. Izraeli, J.W. Harris, O. Navon, Brine inclusions in diamonds: a new upper mantle fluid, Earth Planet. Sci. Lett. 187 (2001) 323–332.
[82] Y.N. Pal'yanov, A.G. Sokol, Y.M. Borzdov, A.F. Khokhryakov, N.V. Sobolev, Diamond formation from mantle carbonate fluids, Nature 400 (1999) 417–418.
[83] M. Akaishi, S. Yamaoka, Crystallization of diamond from C–O–H fluids under high-pressure and high temperature conditions, J. Cryst. Growth 209 (2000) 999–1003.
[84] J.F. Kasting, D.H. Eggler, S.P. Raeburn, Mantle redox evolution and the oxidation state of the Archean atmosphere, J. Geol. 101 (1993) 245–257.
[85] C.E. Melton, A.A. Giardiny, The composition and significance of gas released from natural diamonds from Africa and Brazil, Am. Miner. 59 (1974) 775–782.
[86] R. Rye, H.D. Holland, Paleosoils and the evolution of atmospheric oxygen: a critical review, Am. J. Sci. 298 (1998) 621–672.
[87] M. Bau, R.L. Romer, V. Lüders, N.J. Beukes, Pb, O, and C isotopes in silicified Mooidraai dolomite (Transvaal Supergroup, South Africa): implications for the composition of Paleoproterozoic seawater and 'dating' the increase of oxygen in the Precambrian atmosphere, Earth Planet. Sci. Lett. 174 (1999) 43–57.
[88] J. Farquhar, H. Bao, M. Thiemens, Atmospheric influence of Earth's earliest sulfur cycle, Science 289 (2000) 756–758.
[89] J. Farquhar, B.A. Wing, K.D. McKeegan, J.W. Harris, P. Cartigny, M.A. Thiemens, Mass-independent sulfur of inclusions in diamond and sulfur recycling on early Earth, Science 298 (2002) 2369–2372.
[90] U.H. Wiechert, Earth's early atmosphere, Science 298 (2002) 2341–2342.
[91] P.J. Patchett, N.T. Arndt, Nd isotopes and tectonics of 1.9–1.7 Ga crustal genesis, Earth Planet. Sci. Lett. 78 (1986) 329–338.
[92] S.B. Jacobsen, Isotopic and chemical constraints on mantle–crust evolution, Geochim. Cosmochim. Acta 52 (1988) 1341–1350.
[93] D.J. DePaolo, A.M. Linn, G. Schubert, The continental crustal age distribution: methods of determining mantle separation ages from Sm–Nd isotopic data and application to the southwestern United States, J. Geophys. Res. 96 (1991) 2071–2088.
[94] R.L. Rudnick, Making continental crust, Nature 378 (1995) 571–578.
[95] H.-D. Hensel, M.T. McCulloch, B.W. Chappell, The New England Batholith: constraints on its derivation from Nd and Sr isotopic studies of granitoids and country rocks, Geochim. Cosmochim. Acta 49 (1985) 369–384.
[96] G.W. Eberz, I.A. Nicholls, R. Mass, M.T. McCulloch, D.J. Whiteford, The Nd- and Sr-isotopic composition of I-type microgranitoid enclaves and their host rocks from the Swifts Creek pluton, southeast Australia, Chem. Geol. 85 (1990) 119–134.
[97] C.J. Bryant, R.J. Arculus, B.W. Chappell, Clarence River Supesuite: 250 Ma Cordilleran tonolitic I-type intrusions in eastern Australia, J. Petrol. 38 (1997) 975–1001.
[98] P.L. King, A.J.R. White, B.W. Chappell, C.M. Allen, Characterization and origin of aluminous A-type granites from the Lachlan Fold Belt, southeastern Australia, J. Petrol. 38 (1997) 371–391.
[99] S.D. Samson, W.C. McClelland, P.J. Patchett, G.E. Gehreless, R.G. Anderson, Evidence from neodymium isotopes for mantle contributions to Phanerozoic crustal genesis in the Canadian Cordillera, Nature 337 (1989) 705–709.
[100] D.S. Coleman, T.P. Frost, A.F. Glazner, Evidence from the Lamarck granodiorite for rapid Late Cretaceous crust formation in California, Science 258 (1992) 1924–1926.
[101] D.A. Pickett, J.B. Saleeby, Nd, Sr, and Pb isotopic characteristics of Cretaceous intrusive rocks from deep levels of Sierra Nevada batholith, Tehachapi Mountains, California, Contrib. Mineral. Petrol. 118 (1999) 198–215.
[102] J.B. Whalen, G.A. Jenner, F.J. Longstaffe, F. Robert, C. Gariépy, Geochemical and isotopic (O, Nd, Pb and Sr) constraints on A-type granite petrogenesis based on the Topsails igneous suite, Newfoundland Appalachians, J. Petrol. 37 (6) (1996) 1463–1489.
[103] J. Kinnaird, P. Bowden, African anorogenic alkaline magmatism and mineralization—a discussion with reference to the Niger–Nigerian province, Geol. J. 22 (1987) 297–340.
[104] W. Hildreth, A.N. Halliday, R.L. Christiansen, Isotopic and chemical evidence concerning the genesis and contamination of basaltic and rhyolitic magma beneath the Yellowstone plateau volcanic field, J. Petrol. 32 (1991) 63–138.
[105] S.W. Novak, G.A. Mahood, Rise and fall of a basalt–trachyte–rhyolite magma system at the Kane Springs Wash Caldera, Nevada, Contrib. Mineral. Petrol. 94 (1986) 352–373.
[106] C.D. Frost, B.R. Frost, Reduced rapakivi-type granites: the tholeiite connection, Geology 25 (7) (1997) 647–650.